Probabilistic precipitation analysis in the Central Indus River basin

Paolo Reggiani*, Oleksiy Boyko

Dept. of Civil Engineering, University of Siegen, Germany

Tom H. Rientjes

Dept. of Water Resources, Faculty ITC, University of Twente, Enschede, The Netherlands

Asif Khan

Dept. of Civil Engineering, University of Engineering and Technology, Jalozai Campus, Peshawar, Pakistan

Abstract

Few studies exist on the analysis of precipitation and respective trends during past decades in the Central Indus basin, Pakistans principal river system. One reason for the lack of such studies is data scarcity. Modern-era reanalysis products offer the possibility to fill this gap by delivering simulated precipitation, temperature and other atmospheric variables over poorly monitored areas. Reanalysis products are derived from atmospheric circulation historical re-forecasts, whereby the models are adjusted by means of sequential assimilation of past observations. Despite the fact that these products improve progressively, is essential to post-process to perform systematic bias correction and to asses their predictive uncertainty for specific ground locations. Here we employ six reanalysis products for the Central Indus basin region with the aim to predict basin-average precipitation, detect potential trends and discuss how the suggested approach can be valuable for water resources studies under climate change conditions.

Keywords: Central Indus Basin, Precipitation, Atmospheric reanalysis,

*Corresponding author
Email address: paolo.reggiani@uni-siegen.de (Paolo Reggiani)

1. Introduction

Pakistans national borders enclose a surface area of 880,000 km^2 and a population of approximately 199 million people (2018). In general, the climate is arid, and mean annual precipitation ranges from less than 100 mm in parts of the Lower Indus Plain to over 750 mm in the Upper Indus Plain [1]. The Himalayan foothills however are characterized by heavy precipitation up to 2000 mm and beyond due to orographic effects [2, 3], while the Upper Indus basin is once again dryer, with a mean annual precipitation estimated between 600 and 700 mm [4] . The Indian monsoon advecting moist air from the Bay of Bengal and the Arabian Sea, and the western disturbances, mainly extratropical storms that originate in the Mediterranean and over the Black sea, are the chief sources of rainfall, two-thirds of which usually falls between July and September. On the Punjab plains most of the rain falls during the Monsoons in early July.

Originating on the Tibetan plateau at about 5000 masl., the river Indus flows initially in westerly direction across the Upper Indus Valley, carved in-between the Karakoram range to the North and the Himalayas range to the South, and then exists the mountainous region across a narrow gorge toward the Punjab Plains. The river Indus and its tributaries are the country's most important source of fresh water. With a total drainage area of approximately 1.1 million km^2, the Indus River basin covers approximately 65 % of the territory of Pakistan [5], and extends into neighbouring China, India, and Afghanistan. The Indus river has two main tributaries, the Kabul on the right bank and the Panjnad on the left. The Panjnad is the merged flow of the the Jhelum and Chenab rivers, known as the western rivers together with the river Indus, and the Ravi, Beas and Sutlej, known as the eastern rivers. This division came into effect at the time of settlement of a water dispute between India and Pakistan in 1960 [6]. The closure of the upper part of the Indus basin (UIB) at the Himalayan foothills is marked by Tarbela reservoir, which plays a central role

for Pakistans hydropower production and is the headnode of the large Indus irrigation scheme, one of the largest of its kind.

Due to rapid population growth during recent decades Pakistan has become one among the most water-stressed countries in the world, a situation which eventually is going to approach the status of outright water scarcity [1]. As per 2009 Pakistan had an internal reusable water resources (IRWR) of 323 m^3/inhabitant and year, which is far below 1700 m^3/inhabitant [5], a threshold under which there are indications of water stress. The total available water resources (TAWR) is equally serious with less than 1700 m^3/inhabitant available, slowly approaching a situation of chronic water scarcity once the resource availability has fallen under the 1000 m^3/inhabitant threshold. As at 2010 Pakistan also belongs to the 10 primary groundwater abstracting countries of the world [7, 1] and has severely depleted important aquifers due to unsustainable water mining for irrigation during last decades.

According to assessments by the World Bank [7] there is no feasible intervention at present, which would enable Pakistan to mobilize appreciably more water than it now uses. Pakistans natural dependence on a single major river system means it lacks the robustness in terms of water supply redundancy that most countries enjoy by virtue of drawing water from multiple river basins. To the contrary, Pakistan is also exposed to high risks of floods. As recently as 2010 the country has been hit by an extreme monsoonal rainfall event with extensive flooding in the Punjab and Middle Indus valley, leading to a considerable destruction of infrastructure and crop production with two thousand lives and more than a million homes lost. Another similarly extreme, albeit less harmful flood event occurred in 2011 in the Sindh province, affecting also eastern Balochistan and the southern Punjab with a considerable number of casualties, loss of crop production and property.

In view of long-term highly strained water resources and simultaneous high flood risk in Pakistan, it is of primary importance to correctly asses the spatial distribution of precipitation and related uncertainty for a series of reasons. Firstly, past and present precipitation is a crucial input variable into hydro-

logical decision support tools, for instance rainfall-runoff and flow forecasting models as well as water resources allocation models. For example, incorrect estimation of areal precipitation may lead to erroneous water resources assessments, with potential malinvestments for infrastructure. Secondly, precipitation fields cannot be measured or estimated deterministically, as its space-time structure features a strongly random behaviour. As a result, the uncertainty associated with precipitation estimation or prediction must be accounted for in any decision-making processes for integrated water resources management. The quantification of uncertainty associated with precipitation is also relevant in the case of poorly gauged basins due to lack of sufficiently dense and continuous ground observations for reliable precipitation estimation. Thirdly, hydrometeorological variables such as precipitation, but also temperature and evaporation may be subject to future change and thus require reliable trend quantification by means of climate change indicators [8, 9]. Without probabilistic assessment methods that combine information from multiple predictors (there are currently outputs from more than 20 climate change models available at the CIMP5 portal `https://esgf-node.llnl.gov/search/cmip5/`, which provide the atmospheric modelling basis for the latest IPCC report [10]) such indicators can only be evaluated deterministically, with the risk of misrepresenting possible climate change effects attributable to the uncertainty of projections.

Very few studies on precipitation analysis of relevance for the the Central Indus basin can be found in the literature, despite its high water-related vulnerability. Examples include the interpolated daily precipitation products CRU TS4.01 [11], the GPCC gridded precipitation [12] and APHRODITE [13, 14] datset for the South-East Asian region. In an somewhat different geographical context [15] presented a study on high-altitude monthly precipitation and temperature estimation in the Shigar river basin, Karakoram, Upper Indus, in which six reanalysis products conditioned on a single nearby ground observing station were used. The methodology applied in the analysis is based on a Bayesian processor of uncertainty [16], which combines, and thus maximizes, the compound information on monthly precipitation from numerical precipi-

tation reanalyses, whereby ground observations are used for bias removal and processor calibration. The adopted Bayesian approach is referred to a Model Conditional Processor (MCP) [17] and as such is one of several proven quantitative assessment approaches for uncertainty such as Bayesian Model Averaging (BMA) [18, 19] or Quantile Regression analysis (QR) [20]. Without entering the details on the advantages and disadvantages of different methodological choices, we devote this chapter to a specific application of the Model Conditional Processor (MCP) to the Central Indus basin. Aim of the analysis is the use of six reanalysis products to assess monthly areal precipitation for selected subbasin areas in the Punjab region. In this way we demonstrate the strength of the chosen approach and open the way for further applications of the methodology on uncertainty quantification of hydro-meteorological variables such as precipitation, temperature and evaporation, and specific climate change indicators. The extended goal is to present a method for rational decision support to integrated water-resources planning and infrastructure investments.

The present chapter is structured as follows: In Section 2 we introduce data and methods, in Section 3 we apply the Bayesian processor and present the results, Section 4 is devoted to the discussion of the outcome, while Section 5 contains summary and conclusions. The details of th MCP approach are summarized in the Appendix.

2. Data and methods

2.1. Study area

In this study we focus exclusively on the Central Indus basin, including the subbasins of the Ravi, Jelam, the Upper and Lower Chenab rivers and the Middle Indus valley basin, as depicted in Figure 1. The total study area covers an area of 256462 km^2 and is mostly located in the Pakistani part of the Indus basin, with exception of the Northern Ravi and the Chenab basins reaching into the Indian states of Jammu-Kashmir and Himachal Pradesh. The western fringe of the Middle Indus subbasin lies partly in Afghan territory. The study region is

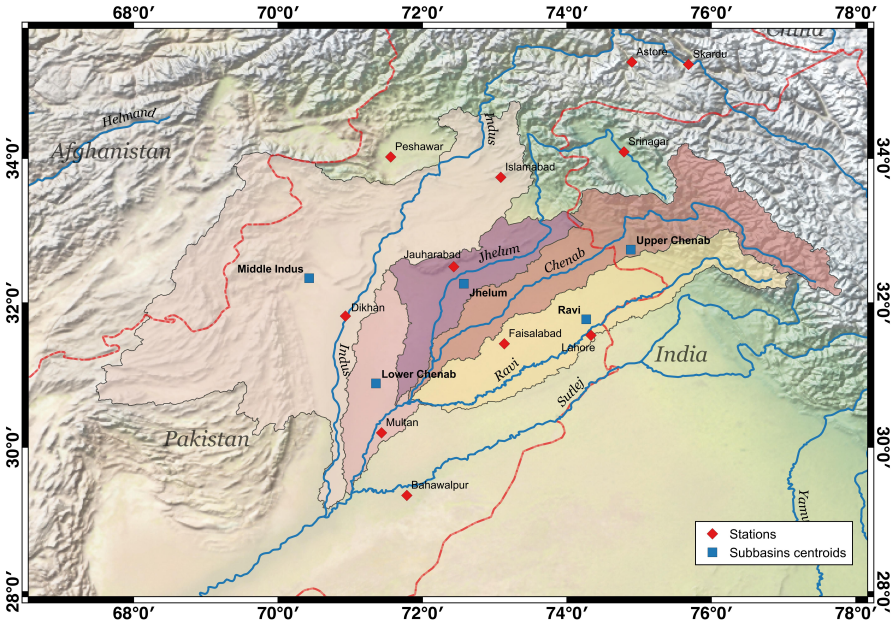

Figure 1: Central Indus study area with subbasin basins and observing stations for precipitation

largely characterized by a near-flat topography in the Pakistani Punjab, while the north-eastern part of Ravi and Chenab reaches into the southern Himalays. Precipitation varies considerably in north-south direction with a maximum mean annual precipitation of 1142 mm recorded in Islamabad, 697 mm in Srinagar, 600 mm in Lahore and falling to a low of 188 mm and 143 mm in Multan and Bahawalpur, respectively. The high precipitation recorded in Islamabad is due to the proximity of the city to the Himalayan foothills, where orographic effects become dominant. Skardu, which is located in the upper Indus valley, also shows precipitation levels of 200 mm, typical for the arid climate found in the low valleys of the Upper Indus basin. **Table 1** summarizes the gauging station network used for this study and the mean annual precipitation recorded at the respective sites. The station positions are also indicated on the map in **Figure 1**.

From an analysis of a regional digital terrain model we extract five subbasins

station	position	elev.	period	P $[mm]$	gaps
Astore	35°20' N, 74°54' E	2394 m	1954-2010	427	0%
Bahawalpur	29°20' N, 71°47' E	110 m	1931-2010	143	0%
D.I.Khan	31°49' N, 70°56' E	171.2 m	1931-2010	269	0%
Faisalabad	31°26' N, 73°08' E	185.5 m	1951-2010	346	0%
Islamabad	33°36' N, 73°05' E	508 m	1976-2010	1142	14%
Jauharabad	32°30' N, 72°26' E	187 m	2007-2010	389	87%
Lahore	31°33' N, 74°20' E	214 m	1931-2010	628	0%
Multan	30°12' N, 71°26' E	121.95 m	1950-2010	188	0%
Peshawar	34°02' N, 71°56' E	372 m	1950-2010	404	3%
Skardu	35°18' N, 75°41' E	2210 m	1952-2010	202	$< 1\%$
Srinagar (IN)	34°05' N, 74°47' E	1587 m	1961-2010	697	0%

Table 1: Position and elevation of recording stations for precipitation, available record length and mean annual precipitation.

(**Figure 1**) making up the study region. Their IDs, centroid position and individual areal extent are summarized in **Table 2**. The area is subject to the influence of the Indian monsoon, which leads to heavy rainfall from June and September, and light rain due to western disturbances between mid-November and mid-February. The region experiences mild spring weather between mid-February to mid-April, which gives way to very hot and dry weather lasting until the onset of the monsoon in the month of June. Temperatures can get close to or exceed 40° C during May and June and fall toward or below the freezing point during December and January, depending on location. In the Himalayas snow is encountered during winter months above the snowfall line.

2.2. In situ observations

The first step in our analysis is the elaboration of the records of monthly cumulative precipitation provided by the Pakistan Meteorological department. The series with original length indicated in **Table 1** were trimmed to the 1979-2010 period selected for the present analysis. Most series were complete with

Subbasin	**centroid**	**area** $[km^2]$
Jhelam	32°15' N, 72°34' E	22046
Middle Indus	32°20' N, 70°25' E	131079
Upper Chenab	32°44' N, 74°53' E	46427
Lower Chenab	30°53' N, 71°21' E	17817
Ravi	31°46' N, 74°16' E	39093

Table 2: Central Indus subbasins used for the precipitation analysis including centroid position and surface area.

only few months missing. The respective percentages of missing values for the 1979-2010 period are indicated in **Table 1**. The most incomplete records are Jauharabad (87 % missing) with only three years of data available, followed by Islamabad (14 % missing) and Peshawar (3 % missing).

To reconstruct smaller dispersed gaps in the records of Islamabad and Lahore we used the statistical procedure described in [21] which is based on multiple linear regression, singular value decomposition and pseudo-expectation-maximization. In this context we used only the record of Lahore to fill the 3-year gap for Islamabad, as the precipitation pattern between the two locations were statistically most similar. Using additional stations with very different precipitation statistics would have distorted the results. Filling the gaps for Peshawar posed no problems at all using all available stations as support.

To fill the 87 % gap in Jauharabad we resorted to Kriging, using all remaining stations as basis. Kriging is a geostatistical method in which the mutual spatial correlation structure of the records is represented by an empirical semi-variogram, which is approximated in terms of a parametric model. One needs to note that the semi-variogram changes each time step and thus needs to be fitted in the present case on a monthly basis. We chose from four different semi-variogram models, which were selected on the basis of optimal weighted least squares fitting [22]. The optimal parameters were found by means of the conjugated gradient method by minimizing the least squares error used as cost function. **Figure 2** shows four semi-variograms and respective paramet-

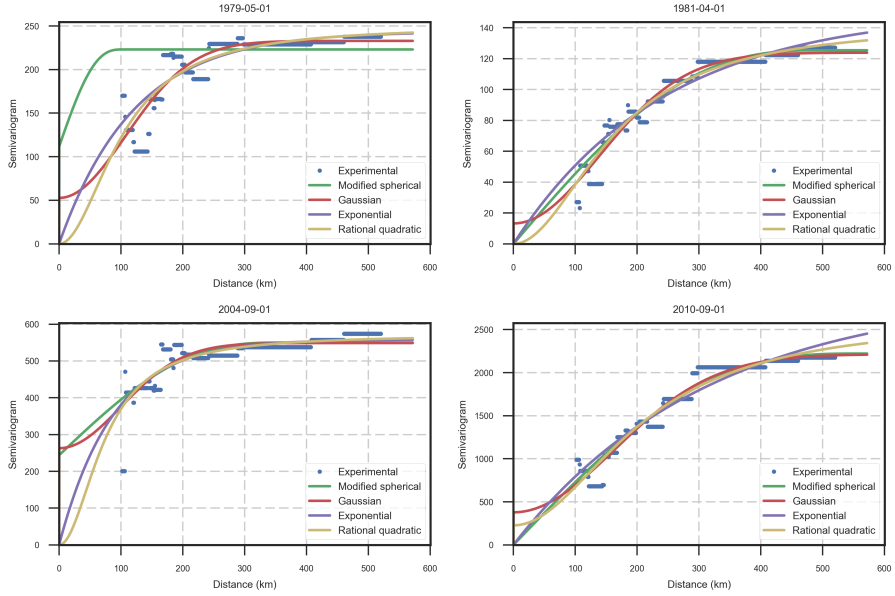

Figure 2: Four empirical and fitted semi variograms for different periods using four fitting models.

ric models (Gaussian, exponential, spherical and rational quadratic model) for four arbitrary months of the study period, that were used for representing the change of variance as a function of the horizontal distance between stations. Once all series were completed, we performed Block-Kriging from the 11 stations in **Table 1** towards the centroids of the subbasins (**Table 2**), obtaining complete estimates of observed monthly areal precipitation in the study basins. These will be used as a reference for comparison with post-processed precipitation from atmospheric reanalysis products. Finally we separated the records for each year into a 5-month sub-record representing the monsoon period (July-November) and a 7-month record representing the inter-monsoon period or dry season (December-May).

2.3. Atmospheric reanalyses

As stated in the Introduction, we resort to an ensemble of six atmospheric reanalyses to be used as predictors for monthly precipitation. We have selected the

most contemporary reanalysis products developed by source organizations which apply different models and data assimilation procedures to obtain a six-member ensemble of independent physically-based estimates of monthly precipitation: 1) ERA-Interim [23], 2) ERA20C [24], 3) Japanese 55-year reanalysis [25], 4) NCEP-NCAR reanalysis R1 [26], 5) NCEP-CFSR [27] and NASA MERRA [28], 6). The products and their most important characteristics are summarized in **Table 3**. For reasons of record length consistency among reanalysis projects, only data from 1979 onwards were used.

Data set	**Origin**	**Grid type**	**Spatial res.**
ERAI	ECMWF	N128 Gaussian	$0.75^\circ \times 0.75^\circ$ ($\sim$ 83 km)
NCEP/NCAR R1	NCEP/ NCAR	$1.875^\circ \times 1.875^\circ$	$1.875^\circ \times 1.875^\circ$ ($\sim$ 209 km)
MERRA	NASA	$1/2^\circ \times 2/3^\circ$	$1/2^\circ \times 2/3^\circ$ ($\sim$ 55 $\times$ 73 km)
NCEP CFSR	NCEP	T382 Gaussian	$0.313^\circ \times 0.313^\circ$ ($\sim$ 38 km)
55Yr Japanese Reanalysis	Jp. Met. Agency	TL390L60	$1.25^\circ \times 1.25^\circ$ ($\sim$ 135 km)
ERA 20C Reanalysis	ECMWF	N80 Gaussian	$1.125^\circ \times 1.125^\circ$ ($\sim$ 125 km)

Table 3: Overview of the six atmospheric reanalyses and gridded observed precipitation indicating the product name, source agency, model grid projection, spatial output resolution for the analysed fields.

Next, the precipitation values for individual model cells are spatially averaged over the five subbasins (**Table 2**, **Figure 1**). The reanalysis outputs have different spatial resolutions and therefore involve a varying number of grid cells. The averaging procedure requires the calculation of weighted mean of the respective variable X using the subbasin mask to identify the relevant model cells. All reanalysis cells that overlap with the area enclosed by the mask are used to perform the averaging. The average $\bar{X}$ is given by the area-weighted

mean precipitation:

$$\bar{X}^j = \frac{\sum_{i=1}^{n} X_i^j \cdot A_i}{A_{tot}} \tag{1}$$

where the index i indicates cell i, j indicates the monthly time step, A_i is the basin area portion covered by the i-th reanalysis pixel, A_{tot} is the subbasin area and n is the total number of cells found within the subbasin mask. The resulting series of basin-average data for each reanalysis series are supposed to hold approximately at the basin centroid.

3. Application of the Model-Conditional Processor

3.1. Predictive uncertainty

Bayesian inference approaches have become increasingly popular in assessing the uncertainty of numerical predictions in flow and weather forecasting, especially after "predictive uncertainty" (PU) was defined [29] as a conditional probability density:

$$PU = f(y|\hat{y}_{1,t_o}, \hat{y}_{2,t_o}, \hat{y}_{3,t_o}, ..., \hat{y}_{n,t_o}) \tag{2}$$

where f is a conditional probability density function, y is the predictand describing an uncertain process such as precipitation at a given time t and $\hat{y}_{i,t_o}, i = 1, ..., n$ are n random predictor variables at time t for a forecast starting at time t_o. In a forecasting context the chief interest lies in the assessment of PU for prediction times $t > t_o$. A reforecast on the other hand, as addressed in this analysis, reproduces the past and thus $t_o = t$ at each time.

The Model-Conditional Processor (MCP) [17] is a probabilistic tool designed to estimate conditional posterior distribution in eq. (2). The prior distributions of both, predictand and predictors, are assumed equal to their climatological distributions and are mapped to the Gaussian space by means of the Normal Quantile Transform (NQT) [30]. In the normal space the interdependency structure of predictand and predictors is assumed multivariate Normal. [16] proposed an extended version of the MCP which allows for the inclusion of multiple forecasting models with heteroscedastic dependency structures. If the assumption

of normality of the multivariate distribution is not acceptable due to significant heteroscedasticity of the residuals in the normal space, the joint distribution of predictand and predictors is separated into multiple truncated normal distributions (TNDs), which are applicable to sub-segments of the normal variable value range. An application of the MCP to monthly precipitation in the Karakoram has been proposed in [15]. Given the prior distributions of predictand and predictors and their joint multivariate normal distribution, Bayes theorem can be applied to derive normal conditional densities of the predictand given multiple predictors. Finally the conditional density is back-transformed from the normal into the original space by inverse NQT. A more detailed mathematical recapitulation of the MCP is provided in the Appendix.

3.2. Normalization of variables

To process the precipitation observations and atmospheric reanalysis data we apply the model-conditional processor in a series of consecutive steps. First we transform the series of monthly basin-average observed precipitation, which were separated into monsoon and dry season into the Gaussian space using the Normal Quantile Transform (NQT). For a realization $\mathbf{y}$ of the random precipitation process $\mathbf{Y}$ consisting of m data points with respective empirical distribution Γ, the NQT is defined as the transformation:

$$\boldsymbol{\eta} = Q^{-1}(\Gamma(\mathbf{y})) \qquad \mathbf{y} = y_k; \quad \boldsymbol{\eta} = \eta_k; \quad k = 1, ..., m \tag{3}$$

where Q^{-1} is the inverse of the standard normal distribution and the transform of $\mathbf{y}$ is denoted with $\boldsymbol{\eta}$ and is $N(0, 1)$. The same is done for the subbasin-average precipitation series of the six atmospheric reanalysis outputs and the CRU observation series, all to be used as indicators. We note that we use monthly precipitation, leading to very few values of zero precipitation in the series. For this reason we model monthly precipitation as a continuous random process with sporadic zero occurrences, in contrast to precipitation at higher temporal resolution, which needs to be modelled as a binary-continuous process

[31] by separating storm from inter-storm periods. This assumption simplifies the following analysis considerably.

3.3. Precipitation: normal distributions

We refer to the notation introduced in Appendix A, which indicates realizations at time t of the standard normal random process $\boldsymbol{\eta}$ and $\hat{\boldsymbol{\eta}}_i$ as η respectively $\hat{\eta}_i, i = 1, ..., n$, whereby we omit an index referring to the time of the realization for notational simplicity. **Figure 3** shows two examples of the NQT-transformed empirical $\eta - \hat{\eta}_i$ relationships as scatterplots for two reanalysis reforecasts (ERAI and JRA) for the monsoon and the dry season respectively in the Jelam subbasins.

One needs to envisage these scatterplots as the projection of the multivariate-normal dependency $(\eta, \hat{\eta}_i), i = 1, ..., n$ onto the respective $\eta - \hat{\eta}_i$ plane as a bivariate-normal process $(\boldsymbol{\eta}, \hat{\boldsymbol{\eta}}_i)$. We note that in all plots there are no data points for the Gaussian variate $\eta < -2.1$ because precipitation is always non-negative. The red solid line indicates the 50% quantile or conditional median obeying to the linear relationship $\eta|\hat{\eta}_i(\hat{\eta}_i) = \rho_{\boldsymbol{\eta}\hat{\boldsymbol{\eta}}^n} \cdot \hat{\eta}_i + \mu_\eta$ with $\mu_\eta = 0$, while conditional mean and variance are equal to:

$$E(\eta|\hat{\eta}_i) = \mu_{\eta|\hat{\eta}_i} = \rho_{\boldsymbol{\eta}\hat{\boldsymbol{\eta}}^n} \cdot \hat{\eta}_i \tag{4}$$

$$Var(\eta|\hat{\eta}_i) = \sigma^2_{\boldsymbol{\eta}|\hat{\boldsymbol{\eta}}_i} = 1 - \rho^2_{\boldsymbol{\eta}\hat{\boldsymbol{\eta}}_i} \tag{5}$$

where $\mu_{\eta|\hat{\eta}_i}$ is the conditional mean and $\rho_{\boldsymbol{\eta}\hat{\boldsymbol{\eta}}_i}$ is the Pearson correlation. We note that thanks to the transformation of original data into standard normal variates $N(0, 1)$ the Pearson correlation is equal to the covariance and the conditional median coincides with conditional mean and modal values. The red dash-dotted lines indicate the 95% credible interval and are at a parallel distance of two standard deviations from the mean. The parametric conditional multivariate normal density function for a single predictor $\hat{\eta}_i$ is given by the expression:

$$\phi(\eta|\hat{\eta}_i) = \frac{exp[-\frac{1}{2}(\eta - \mu_{\eta|\hat{\eta}_i})^2/(1 - \rho^2_{\boldsymbol{\eta}\hat{\boldsymbol{\eta}}_i})]}{\sqrt{2\pi \cdot (1 - \rho^2_{\boldsymbol{\eta}\hat{\boldsymbol{\eta}}_i})}} \tag{6}$$

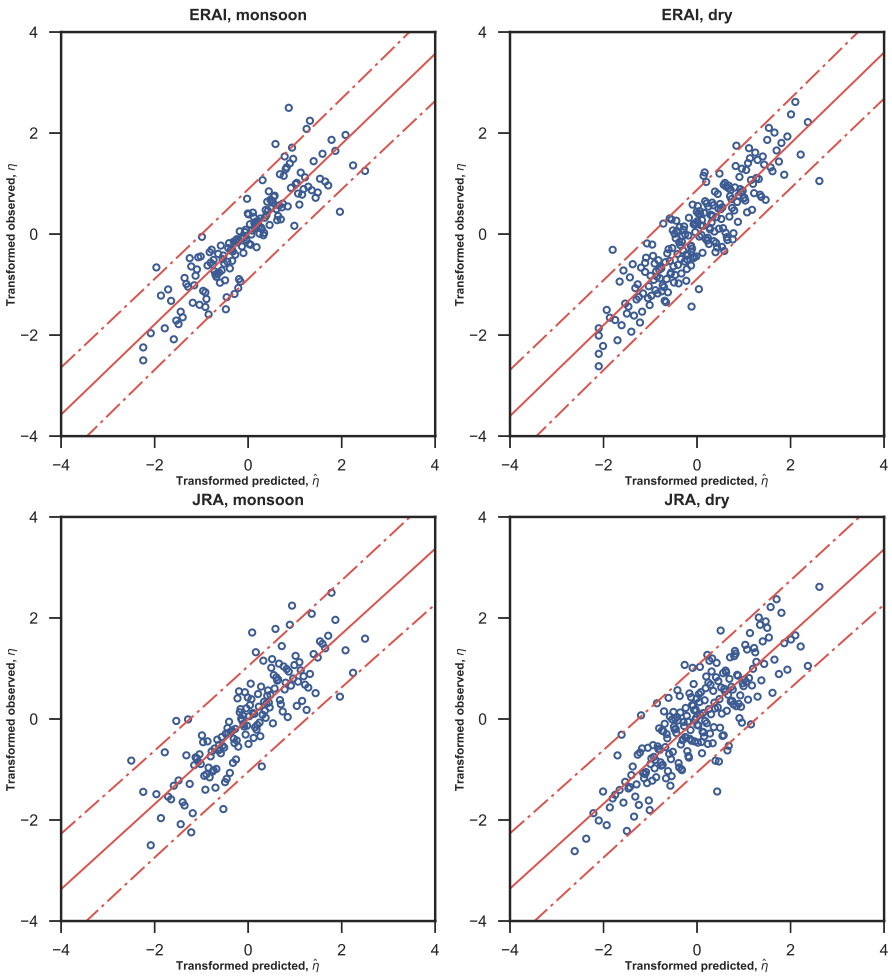

Figure 3: Jhelam subbasin: scatterplots and regression line showing the linear dependency between predictand and predictor for ERAI (top) and JRA (bottom) reanalysis, monsoon (left) and dry period (right).

We note that the conditional variance $\sigma^2_{\boldsymbol{\eta}|\hat{\boldsymbol{\eta}}_i} = (1 - \rho^2_{\boldsymbol{\eta}\hat{\boldsymbol{\eta}}_i})$ is at the denominator and thus with $\rho_{\boldsymbol{\eta}\hat{\boldsymbol{\eta}}_i} \to 1$ and $\sigma^2_{\boldsymbol{\eta}|\hat{\boldsymbol{\eta}}_i} \to 0$ the conditional density curve becomes steeper with probability mass narrowly concentrated. This is tantamount to minimizing the predictive uncertainty by using an increasingly "optimal" model. As described in more detail in the Appendix, the conditional density can be extended to include multiple predictors as conditioning variables, leading to the following parametric multi-normal density function of η, conditional on n potential predictors:

$$\phi(\eta|\hat{\eta}_1, ..., \hat{\eta}_n) = \frac{exp[-\frac{1}{2}(\eta - \mu_{\eta|\hat{\eta}^n})^2/\sigma^2_{\boldsymbol{\eta}|\hat{\boldsymbol{\eta}}^n}]}{\sqrt{2\pi} \cdot \sigma_{\boldsymbol{\eta}|\hat{\boldsymbol{\eta}}^n}} \tag{7}$$

where conditional mean and variance are expressed in terms of the $(n+1) \times (n+1)$-dimensional variance-covariance matrix $\boldsymbol{C}_{\boldsymbol{\eta}.\hat{\boldsymbol{\eta}}^n}$ with sub-matrices $\boldsymbol{C}_{\boldsymbol{\eta}\hat{\boldsymbol{\eta}}^n}$ and $\boldsymbol{C}_{\hat{\boldsymbol{\eta}}^n\hat{\boldsymbol{\eta}}^n}$:

$$\mu_{\eta|\hat{\eta}^n} = \boldsymbol{C}_{\boldsymbol{\eta}\hat{\boldsymbol{\eta}}^n} \cdot \boldsymbol{C}^{-\mathbf{1}}_{\hat{\boldsymbol{\eta}}^n\hat{\boldsymbol{\eta}}^n} \cdot \hat{\eta}^n \tag{8}$$

$$\sigma^2_{\boldsymbol{\eta}|\hat{\boldsymbol{\eta}}^n} = 1 - \boldsymbol{C}_{\boldsymbol{\eta}\hat{\boldsymbol{\eta}}^n} \cdot \boldsymbol{C}^{-\mathbf{1}}_{\hat{\boldsymbol{\eta}}^n\hat{\boldsymbol{\eta}}^n} \cdot \boldsymbol{C}^T_{\boldsymbol{\eta}\hat{\boldsymbol{\eta}}^n} \tag{9}$$

In Eq. (7) the variance-covariance matrix combines n different models with observations. The covariances are evaluated over a sufficiently long calibration period, for which predictions as well as observations are available, and specify the added value of the different forecast models by weighting the predictor values at a given time $\hat{\eta}^n$ accordingly in the conditional variance $\sigma^2_{\boldsymbol{\eta}|\hat{\boldsymbol{\eta}}^n}$. Model forecasts that correlate poorly with the predictand are weighted lower with respect to those with higher correlation. Eq. (7) is the conditional of the multi-variate normal density $\phi(\eta, \hat{\eta}_1, ..., \hat{\eta}_n)$ defined in an $(n+1)$-dimensional data space. Assuming a homoscedastic dependence structure $(\eta, \hat{\eta}_i)$ between variables, Eqns. (7), (8) and (9) hold over the entire value range of $\hat{\eta}_i$. However, in a situation of heteroscedastic dependency it may become necessary to derive separate dependence structures for two or multiple subintervals of the $\hat{\eta}_i$ value range. For the purpose of the present case study we proceed assuming homoscedatic dependencies.

3.4. Backtransformation into the orignal space

Once the series of conditional means and the 95% confidence intervals of the conditional densities have been obtained in the Gaussian space, the normal variates need to be back-transformed into the real space. This is achieved by inverting the NQT (3):

$$\mathbf{y}|\hat{\mathbf{y}} = \Gamma^{-1}(Q(\boldsymbol{\eta}|\hat{\boldsymbol{\eta}})) \qquad \mathbf{y} = y_k, \boldsymbol{\eta} = \eta_k; k = 1, ..., m \tag{10}$$

For this purpose the empirical cumulative distribution function Γ, which is monotonically ascending, is interpolated by means of piecewise linear segments, while the distribution tails below the 15% and above the 85% quantile are modelled with a Pareto distribution. Approximating the tails with Pareto distributions ensures a smooth back-transformation of the extreme high and low range of the standard normal precipitation variate for extreme events. For example, in the very high precipitation range, inaccurate modelling of the distribution tails can cause large deviations of back-transformed precipitation from actual values for small in the Gaussian variate, leading inevitably to distorted estimation of the conditional mean and the credibility intervals in the original space.

4. Application and results

4.1. Calibration

First we calibrate the processor for the Central Indus region by applying it to the precipitation series for the centroids of the five subbasins. For calibration we select the 26-year period form 1979-2005. The results of the post-processed reanalysis data for the calibration period and the five subbasins in **Table 2** is shown in the subplots of **Figure 5**. The figure depicts the MCP-processed and combined monthly reanalysis data for 1979-2005. The processor performs bias-removal and returns estimates of the observed precipitation at the subbasin centroids in terms of the expected value of the back-transformed conditional density (9), i.e the conditional mean. The navy blue line in the figures represents the observed areal average monthly values at the centroid, while the

red line is the conditional mean estimating the monthly precipitation given n reanalysis precipitation values as reforecast predictors. The dark and light grey shaded areas represent the 50% and 95% confidence intervals, respectively. In other words, given multiple predictions of the mean monthly basin-average precipitation, the processor returns at each time step a probability density function indicating the probability mass distribution and uncertainty bandwidth for actual precipitation. The calibrated processor can be utilized in forecast mode to estimate monthly mean areal precipitation given multiple forecasts.

4.2. Performance indicators

The performance of the processor can be be examined on hand of a series of indicators evaluated in the normal space, which quantify the skill of each single prediction and the Bayesian combination of all predictions. A first quantitative indicator of performance is the intercomparison of the correlations of observed and predicted monthly means. A more in-depth analysis of processor performance can be obtained by looking at the correlation and variance of the residuals. **Table 4** and **Table 5** show an overview of the correlations (first row), the variance of the residuals (also called variance unexplained) and the variance explained (second and third row) for the postprocessing of the Jehlam subbasin data, monsoon and dry season respectively. The first type of variance is an overall indicator of the Gaussian scatter around the linear regression model indicated in **Figure 3**, while the latter is the variance, which can be explained solely by the regression model. In addition we calculate the fractions of variance explained and variance unexplained with respect to total variance (fourth and fifth row), to show the percentages of each. As can be seen in the tables, all six models have a correlation with observations between 0.62 and 0.89 over both seasons. The combination of all models (first row, last column) increases the correlations to a value > 0.9 for both seasons, proving that there is net added informative value in performing a Bayesian combination of multiple predictors. However, the fraction of variance unexplained varies between 0.8% down to 21% of total variance, indicating that precipitation prediction is clearly much better

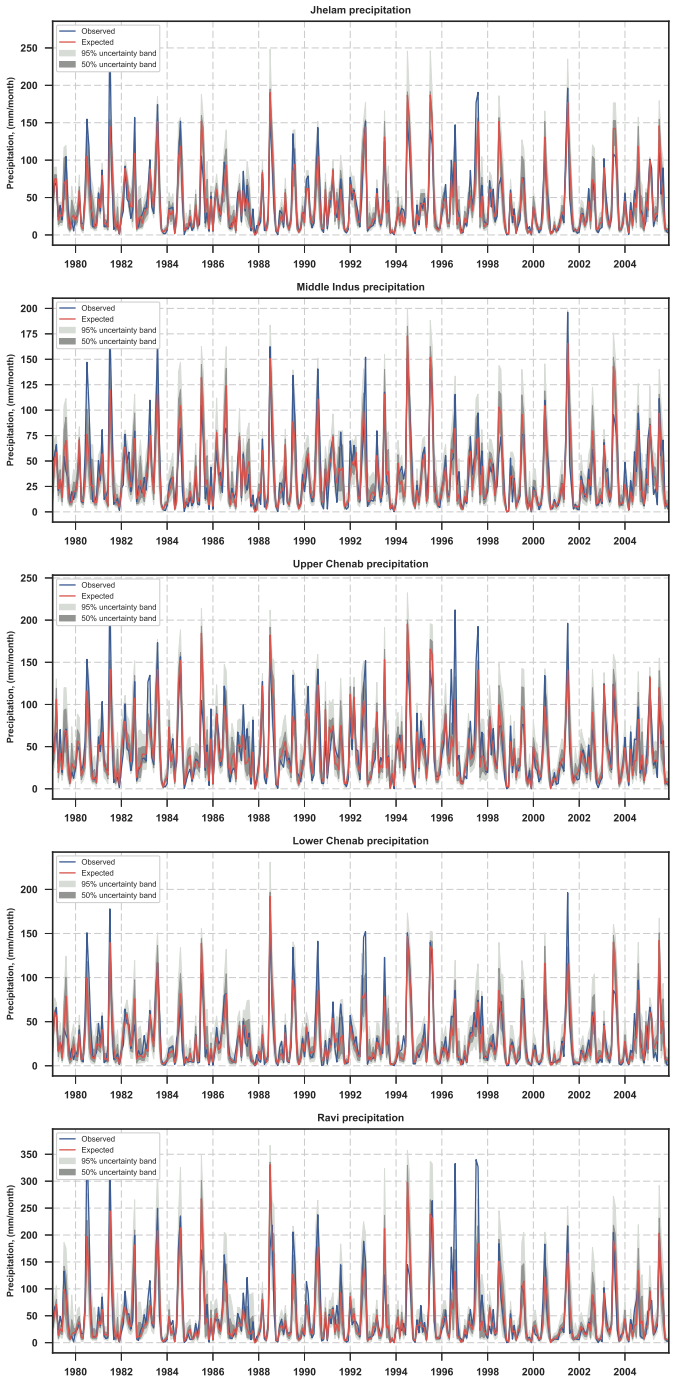

Figure 4: Processor calibration 1979-2005: conditional mean, confidence intervals and precipitation observed for the five subbasins of the study area.

by some models (ERAI, JRA and MERRA) than the remaining ones (ERA20, CFSR, NCAR R1) and is highest when combining all models (fourth row, last column) .

Next we report the "signal-to-noise" ratio (sixt row), a decision-theoretic measure of informativeness of output [29] for individual models and the combination of all models. It shows values that are smallest for ERA20C, R1 and CFSR and highest for JRA55, ERAI and MERRA. The combination of all models brings the ratio to a value of 4.77 for the monsson season and 3.69 for the dry season, indicating that the co-processing of all models leads to an improvement of several times with respect to the worst performing predictor when processed as a single model. In the hypothetical case of a totally uninformative model, which would be completely uncorrelated with observations, i.e. $\rho_{\eta\hat{\eta}_i} = 0$, the total variance becomes unexplained and the signal-to-noise ratio $\rho^2_{\eta\hat{\eta}_i}/(1-\rho^2_{\eta\hat{\eta}_i})$ drops to zero. To the contrary if the model is "perfect", $\rho_{\eta\hat{\eta}_i} = 1$ and the signal-to-noise ratio $\rightarrow \infty$. The bias and RMSE, both calculated on the backtransformed variables, are reported in rows 6 and 7. We note that before processing the reanalysis data are significantly biased, while bias has been removed after processing and combining all reanalysess. The last row reports the RMSE between observations and conditional means.

Finally in **Table 6** we show a summary of the correlations observations-model for individual models and subbasins before the processing and after Bayesian combination of all models. We note that the correlations before processing are in the range between 0.52 - 0.86 and increases to a value of 0.9 after processing, when correlating the conditional mean with observations.

4.3. Validation

Finally we validate the calibrated processor on the 2006-2010 period by using the reanalysis output as a predictor and estimating the actual precipitation through the conditional mean value. As we are working in the past, we can compare directly the processor output with the observations. The results of the processor run for the validation period are shown in **Figure 5**. We note

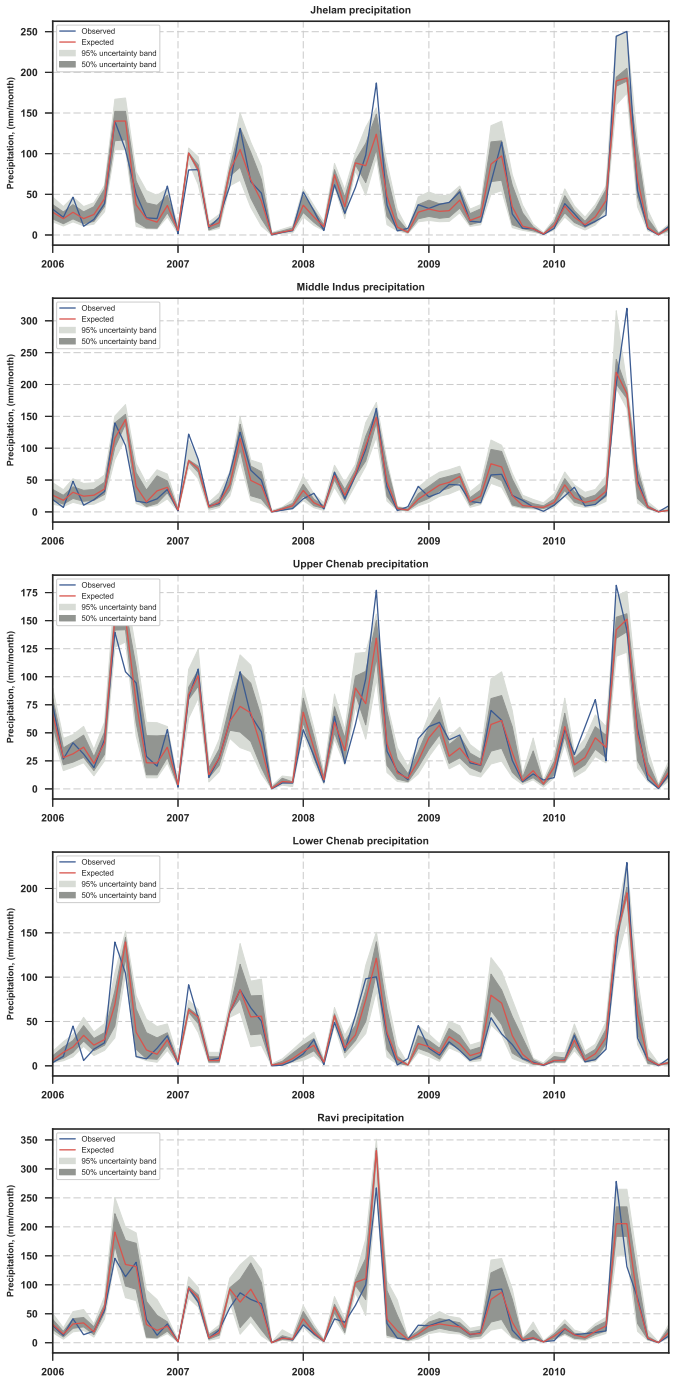

Figure 5: Processor validation 2006-2010: conditional mean, confidence intervals and precipitation observed for the five subbasins of the study area.

that the observations lie mostly within the 95% confidence interval and also the precipitation event of 2010, which caused the large Indus floods, is captured as lying on the upper fringe of the 95% confidence interval. Even though this event was not included in the calibration period, the processor managed to identify it as probable on the basis of the six reanalysis predictions.

5. Summary and Conclusions

In this study Bayesian inference was applied to quantitatively assess the uncertainty of monthly precipitation for five subbasins in the Central Indus region using a six-member ensemble of independent reanalysis outputs. A probabilistic processor was calibrated on the 1979-2005 year period and applied in validation mode for the 2006-2010. In the validation period the reanalysis was used as a pseudo-forecast to show the capabilities of the method in predicting the basin-average precipitation and respective uncertainty, expressed in terms of confidence intervals. This methodology has been applied for the first time in the Upper Indus basin, Pakistan [15], to quantify precipitation uncertainty for a poorly gauged area in the Karakoram and has now been extended to the Central Indus region. The strength of the methodology lies in the possibility to use the processes to perform educated estimation of areal precipitation, including related uncertainty, by making use of multiple predictors. Such probabilistic estimates of precipitation are of considerable importance for future water allocation analysis and the planning of infrastructure and related investments. While we used reanalysis products as predictors in the current example, these can be extended to satellite or radar precipitation estimates or involve different predictors such as relative air humidity. The present methodology can also be employed to perform an analysis of precipitation, temperature or evaporation forecasts from climate projections, which can be used in the same fashion as reanalysis products in the present example. Climate model performance on historical data can be evaluated over a historical periods and the calibrated probabilistic processor adapted to perform predictions for the mid-21st century

and beyond.

6. Acknowledgements

Special thanks go to the Pakistan Meteorological Department, which has provided the precipitation data. Without their support this research would not have been possible. We also acknowledge the organizations and the teams responsible for the creation and publication of the JRA55, NCEP-NCAR (R1), NCEP-CFSR, ERA20C, ERA-Interim and MERRA reanalysis archives. The JRA55 data were obtained from the Japan Meteorological Agency (`http://jra.kishou.go.jp`), NCEP-NCAR (R1) data were obtained from NOAA/OAR/ESRL PSD (`http://www.esrl.noaa.gov/psd`), NCEP-CFSR data from NOAA (`http://cfs.ncep.noaa.gov/cfsr/`), ERA 20th Century and ERA-Interim reanalysis data from ECMWF (`http://www.ecmwf.int/en/research/climate-reanalysis`) and Modern-Era Retrospective Reanalysis (MERRA) data from NASA (`http://gmao.gsfc.nasa.gov/research/merra/`).

References

[1] The United Nations world water development report 4: Managing Water under Uncertainty and Risk, Technical Report, UNESCO, Paris, 2012.

[2] P. Singh, N. Kumar, Effect of orography on precipitation in the western Himalayan region, Hydrology and Earth Systems Sciences 199 (1997) 183–206.

[3] D. R. Archer, H. J. Fowler, Spatial and temporal variations in precipitation in the upper indus basin, global teleconnections and hydrological implications, Hydrol. Earth Sys. Sci. 8 (2003) 47–61.

[4] P. Reggiani, T. H. M. Rientjes, A reflection on the long-term water balance of the upper indus basin, Hydrol. Res. 46 (2015) 446–462.

[5] Irrigation in Southern and Eastern Asia in figures, Technical Report 44375, FAO, Rome, 2011.

[6] N. D. Gulhati, The Indus Waters Treaty: An Exercise in International Mediation, Allied Publishers, Bombay, 1973.

[7] Water Security in Pakistan: Issues and Challenges, Technical Report, United Nations Development Programme Pakistan, Islamabad, Pakistan, 2016.

[8] A. Sankarasubramanian, R. M. Vogel, J. F. Limbrunner, Climate elasticity of streamflow in the united states, Water Resour. Res. 37 (2001) 1771–1781.

[9] P. A. Ray, C. M. Brown, Confronting Climate Uncertainty in Water Resources Planning and Project Design The Decision Tree Framework, Technical Report 99180, The World Bank Group, Washington D.C., 2015.

[10] Climate Change 2014: Synthesis Report. Contribution of Working Groups I, II and III to the Fifth Assessment Report of the Intergovernmental Panel on Climate Change, Technical Report, IPCC, Geneva, Switzerland, 2014.

[11] I. Harris, P. D. Jones, T. J. Osborn, D. H. Lister, Updated high-resolution grids of monthly climatic observations—the cru ts3.10 dataset, Int. J. Climatol. 34 (2013) 623–642.

[12] U. Schneider, A. Becker, P. Finger, A. Meyer-Christoffer, M. Ziese, B. Rudolf, Gpcc's new land surface precipitation climatology based on quality-controlled in situ data and its role in quantifying the global water cycle, Theor. Appl. Climatol. 115 (2014) 15–40.

[13] A. Yatagai, O. Arakawa, K. Kamiguchi, H. Kawamoto, M. I. Nodzu, A. Hamada, Aphrodite: Constructing a long-term daily gridded precipitation dataset for asia based on a dense network of rain gauges, Bull. Amer. Meteor. Soc. 93 (2012) 1401–1415.

[14] G. Ali, G. Rasul, T. Mahmood, Q. Zaman, S. B. Cheema, Validation of aphrodite precipitation data for humid and sub humid regions of pakistan, Pakistan Journal of Meteorology 9 (2012) 57–69.

[15] P. Reggiani, G. Coccia, B. Mukhopadhyay, Predictive uncertainty estimation on a precipitation and temperature reanalysis ensemble for shigar basin, central karakoram, Water 8 (2016) 263.

[16] G. Coccia, E. Todini, Recent developments in predictive uncertainty assessment based on the model conditional processor approach, Hydrol. and Earth Syst. Sci. 15 (2011) 3253–3274.

[17] E. Todini, A model conditional processor to assess predictive uncertainty in flood forecasting, Int. J. of River Basin Management 36 (2008) 3265–3277.

[18] A. E. Raftery, Bayesian model selection in structural equation models, in k. a. bollen and j. s. long (eds.), Testing Structural Equation Modelsv (1993) 163–180.

[19] A. E. Raftery, T. Gneiting, F. Balabdaoui, M. Polakowski, Using bayesian model averaging to calibrate forecast ensembles, Monthy Weather Review 133 (2005) 1155–1174.

[20] R. Koenker, Quantile Regression, Econometric Society Monographs, Cambridge University Press, 2005.

[21] G. Pegram, Patching rainfall data using regression methods. 3. grouping, patching and outlier detection, J. of Hydrol. 198 (1997) 319–334.

[22] N. Cressie, Fitting variogram models by weighted least squares, Mathematical Geology, Vol. 17, No. 5, 1985 17 (1985) 663–586.

[23] D. P. Dee, M. Balmaseda, G. Balsamo, R. Engelen, A. J. Simmons, J. N. Thepaut, Toward a consistent reanalysis of the climate system, Bull. Amer. Meteor. Soc. 95 (2014) 1235–1248.

[24] A. Stickler, S. Brönnimann, M. A. Valente, J. Bethke, A. Sterin, S. Jourdain, E. Roucaute, M. V. Vasquez, D. A. Reyes, R. Allan, D. Dee, Era-clim: Historical surface and upper-air data for future reanalyses, Bull. Amer. Meteor. Soc. 95 (2010) 1419–1430.

[25] S. Kobayashi, Y. Ota, Y. Harada, A. Ebita, M. Moriya, H. Onoda, K. Onogi, H. Kamahori, C. Kobayashi, H. Endo, K. Miyaoka, K. Takahashi, The jra-55 reanalysis: General specifications and basic characteristics, J. Met. Soc. Jap. 93 (2015) 5–48.

[26] R. Kistler, E. Kalnay, W. Collins, S. Saha, G. White, J. Woollen, M. Chelliah, W. Ebisuzaki, M. Kanamitsu, V. Kousky, H. van den Dool, R. Jenne, M. Fiorino, The ncep-ncar 50-year reanalysis: Monthly means cd-rom and documentation, Bull. Amer. Meteor. Soc. 82 (2001) 247–267.

[27] S. S. et. al., The ncep climate forecast system reanalysis, Bull. Amer. Meteor. Soc. 91 (2010) 1015–1057.

[28] M. M. Rienecker, M. J. Suarez, R. Gelaro, R. Todling, J. Bacmeister, E. Liu, M. G. Bosilovich, S. D. Schubert, L. Takacs, G. K. Kim, S. Bloom, J. Chen, D. Collins, A. Conaty, A. da Silva, W. Gu, J. Joiner, R. D. Koster, R. Lucchesi, A. Molod, T. Owens, S. Pawson, P. Pegion, C. R. Redder, R. Reichle, F. R. Robertson, A. G. Ruddick, M. Sienkiewicz, J. Woolle, Merra: Nasa's modern-era retrospective analysis for research and applications, J. Clim. 24 (2011) 3624–3648.

[29] R. Krzysztofowicz, Bayesian theory of probabilistic forecasting via deterministic hydrologic model, Water Resour. Res. 35 (1999) 2739–2750.

[30] D. S. Wilks, Statistical Methods in the Atmospheric Sciences: An Introduction, Academic Press, 1995.

[31] R. Krzysztofowicz, K. S. Kelly, Hydrologic uncertainty processor for probabilistic river stage forecasting, Water Resour. Res. 36 (2000) 3265–3277.

[32] K. V. Mardia, J. T. Kent, J. M. Bibby, Multivariate Analysis. Probability and Mathematical Statistics, Academic Press, London, 1979.

List of Figures

1 Central Indus study area with subbasin basins and observing stations for precipitation 6

2 Four empirical and fitted semi variograms for different periods using four fitting models. 9

3 Jhelam subbasin: scatterplots and regression line showing the linear dependency between predictand and predictor for ERAI (top) and JRA (bottom) reanalysis, monsoon (left) and dry period (right). 14

4 Processor calibration 1979-2005: conditional mean, confidence intervals and precipitation observed for the five subbasins of the study area. 18

5 Processor validation 2006-2010: conditional mean, confidence intervals and precipitation observed for the five subbasins of the study area. 20

List of Tables

1 Position and elevation of recording stations for precipitation, available record length and mean annual precipitation. 7

2 Central Indus subbasins used for the precipitation analysis including centroid position and surface area. 8

3 Overview of the six atmospheric reanalyses and gridded observed precipitation indicating the product name, source agency, model grid projection, spatial output resolution for the analysed fields. . 10

4 Jhelam, 1979-2005, monsoon season: summary of performance indicators after uncertainty processing for individual models and the combination of all models. 31

5 Jhelam, 1979-2005, dry season: summary of performance indicators after uncertainty processing for individual models and the combination of all models. 31

6 Correlations between observations vs. raw predictions ($corr(y, \hat{y}_i)$) and observations vs. posterior conditional mean ($corr(y, E[\mathbf{y}|\hat{\mathbf{y}}^{\mathbf{n}}])$). 32

Appendix A. The Model Conditional processor

The Model Conditional Processor (MCP) has been first presented [17] in the context of flood forecasting as a Bayesian uncertainty processor which uses the output of a single forecasting model for water levels or flows to estimate the predictive uncertainty (PU) on respective values to be observed:

$$PU = f(\mathbf{y}|\hat{\mathbf{y}}) \tag{A.1}$$

where f is a conditional probability density function, $\mathbf{y}$ is the random time series vector of observations which is to be predicted, and $\hat{\mathbf{y}}$ the random model output vector acting as predictor. The empirical probability distributions of predictand and predictor can be mapped into the normal space by applying the non-parametric Normal Quantile Transform (NQT) [30]. The transformed standard normal variables, $N(0,1)$, are indicated with $\boldsymbol{\eta}$ and $\hat{\boldsymbol{\eta}}$, and can be modelled by respective parametric expressions of normal distributions. In the normal space the joint distribution of the two variables, $\Phi(\boldsymbol{\eta}, \hat{\boldsymbol{\eta}})$ is bivariate normal for which the conditional density $\phi(\boldsymbol{\eta}|\hat{\boldsymbol{\eta}})$ can be evaluated analytically. The conditional density can later be back-transformed from the normal to the original space, giving the the predictive uncertainty (A.1).

The single-model case can be extended by analogy to include multiple models as predictors [16]. Based on the properties of the multivariate normal distribution [32], the MCP allows to evaluate the density of the predictand conditional on the forecasts by n models via multiple regression in the normal space.

The derivation of the predictive density is performed by first converting observations $\mathbf{y}$ and the forecasts by the n prediction models, $\hat{\mathbf{y}}^n = (\hat{\mathbf{y}}_1, \hat{\mathbf{y}}_2, ..., \hat{\mathbf{y}}_n)$, into the Gaussian space by NQT. The transformed variables are denoted with the Greek letter $\boldsymbol{\eta}$. If m is the number of data in the observed series, $\mathbf{y}$ and its transform $\boldsymbol{\eta}$ are vectors of length m, while the predictions $\hat{\mathbf{y}}^n$ and their respective transforms $\hat{\boldsymbol{\eta}}^n$ are organized in $m \times n$ matrices. In the normal space predictand and predictor are related through a joint probability distribution with vector of means $\boldsymbol{\mu}_{\boldsymbol{\eta},\hat{\boldsymbol{\eta}}^n}$ and variance-covariance matrix $\boldsymbol{C}_{\boldsymbol{\eta},\hat{\boldsymbol{\eta}}^n}$. Because the

transformed variables are standard normal, the vector of means of the ensemble of variables (observations and predictors) is equal to the null vector:

$$\boldsymbol{\mu}_{\boldsymbol{\eta},\hat{\boldsymbol{\eta}}^n} = \begin{bmatrix} 0 \\ \vdots \\ 0 \end{bmatrix} \tag{A.2}$$

while the variance-covariance matrix is structured as follows:

$$\boldsymbol{C}_{\boldsymbol{\eta},\hat{\boldsymbol{\eta}}^n} = \begin{bmatrix} \boldsymbol{C}_{\boldsymbol{\eta}\boldsymbol{\eta}} & \boldsymbol{C}_{\boldsymbol{\eta}\hat{\boldsymbol{\eta}}^n} \\ \boldsymbol{C}^T_{\boldsymbol{\eta}\hat{\boldsymbol{\eta}}^n} & \boldsymbol{C}_{\hat{\boldsymbol{\eta}}^n\hat{\boldsymbol{\eta}}^n} \end{bmatrix} \tag{A.3}$$

Moreover, as the standard normal variance is equal to 1, the covariances coincide with the Pearson product moment correlations between the variables, and can be interpreted as slopes of the linear regressions between variables. Consequently $\boldsymbol{C}_{\boldsymbol{\eta}\boldsymbol{\eta}} = 1$, $\boldsymbol{C}_{\boldsymbol{\eta}\hat{\boldsymbol{\eta}}^n} = [\boldsymbol{\rho}_{\boldsymbol{\eta}\hat{\boldsymbol{\eta}}_1}, \ldots, \boldsymbol{\rho}_{\boldsymbol{\eta}\hat{\boldsymbol{\eta}}_n}]$ is a $1 \times n$ vector of correlations, while:

$$\boldsymbol{C}_{\hat{\boldsymbol{\eta}}^n\hat{\boldsymbol{\eta}}^n} = \begin{bmatrix} 1 & \boldsymbol{\rho}_{\hat{\boldsymbol{\eta}}_1\hat{\boldsymbol{\eta}}_2} & \cdots & \boldsymbol{\rho}_{\hat{\boldsymbol{\eta}}_1\hat{\boldsymbol{\eta}}_n} \\ \boldsymbol{\rho}_{\hat{\boldsymbol{\eta}}_2\hat{\boldsymbol{\eta}}_1} & \ddots & \ddots & \vdots \\ \vdots & \ddots & \ddots & \boldsymbol{\rho}_{\hat{\boldsymbol{\eta}}_{n-1}\hat{\boldsymbol{\eta}}_n} \\ \boldsymbol{\rho}_{\hat{\boldsymbol{\eta}}_n\hat{\boldsymbol{\eta}}_1} & \cdots & \boldsymbol{\rho}_{\hat{\boldsymbol{\eta}}_n\hat{\boldsymbol{\eta}}_{n-1}} & 1 \end{bmatrix} \tag{A.4}$$

is a $n \times n$ matrix of correlations. The joint observations-forecast probability density is the multi-variate normal density:

$$\phi(\boldsymbol{\eta}, \hat{\boldsymbol{\eta}}^n) = \frac{exp(-\frac{1}{2} \cdot [(\boldsymbol{\eta}, \hat{\boldsymbol{\eta}}^n) - \boldsymbol{\mu}_{\boldsymbol{\eta},\hat{\boldsymbol{\eta}}^n}]^T \cdot \boldsymbol{C}^{-1}_{\boldsymbol{\eta},\hat{\boldsymbol{\eta}}^n} \cdot [(\boldsymbol{\eta}, \hat{\boldsymbol{\eta}}^n) - \boldsymbol{\mu}_{\boldsymbol{\eta},\hat{\boldsymbol{\eta}}^n}])}{\sqrt{(2\pi)^{(n+1)} \cdot |\boldsymbol{C}_{\boldsymbol{\eta},\hat{\boldsymbol{\eta}}^n}|}} \tag{A.5}$$

from which we obtain an analytical expression of the conditional density by exploiting the properties of the multi-variate normal distributions [32] and dividing by the marginal density:

$$\phi(\boldsymbol{\eta}|\hat{\boldsymbol{\eta}}^n) = \frac{\phi(\boldsymbol{\eta}, \hat{\boldsymbol{\eta}}^n)}{\phi(\hat{\boldsymbol{\eta}}^n)} = \frac{\phi(\boldsymbol{\eta}, \hat{\boldsymbol{\eta}}^n)}{\int_{-\infty}^{\infty} \phi(\boldsymbol{\eta}, \hat{\boldsymbol{\eta}}^n)\, \phi(\boldsymbol{\eta})\, d\boldsymbol{\eta}} = \frac{exp[-\frac{1}{2}(\boldsymbol{\eta} - \boldsymbol{\mu}_{\boldsymbol{\eta}|\hat{\boldsymbol{\eta}}^n})^2/\sigma^2_{\boldsymbol{\eta}|\hat{\boldsymbol{\eta}}^n}]}{\sqrt{2\pi} \cdot \sigma_{\boldsymbol{\eta}|\hat{\boldsymbol{\eta}}^n}} \tag{A.6}$$

where mean and variance of the conditional density are as follows:

$$\boldsymbol{\mu}_{\boldsymbol{\eta}|\hat{\boldsymbol{\eta}}^n} = \boldsymbol{C}_{\boldsymbol{\eta}\hat{\boldsymbol{\eta}}^n} \cdot \boldsymbol{C}^{-\mathbf{1}}_{\hat{\boldsymbol{\eta}}^n\hat{\boldsymbol{\eta}}^n} \cdot \hat{\boldsymbol{\eta}}^{n\,T} \tag{A.7}$$

$$\sigma^2_{\boldsymbol{\eta}|\hat{\boldsymbol{\eta}}^n} = 1 - \boldsymbol{C}_{\boldsymbol{\eta}\hat{\boldsymbol{\eta}}^n} \cdot \boldsymbol{C}^{-\mathbf{1}}_{\hat{\boldsymbol{\eta}}^n\hat{\boldsymbol{\eta}}^n} \cdot \boldsymbol{C}^T_{\boldsymbol{\eta}\hat{\boldsymbol{\eta}}^n} \tag{A.8}$$

We observe that Eqns. (A.5), (A.6) and (A.7) are vectorial with each vector position referring to a given observing and prediction time t. The predictive density at time t can be obtained by evaluating the respective expressions for realizations of the random observations $\boldsymbol{\eta}$ and model forecasts $\hat{\boldsymbol{\eta}}^{\boldsymbol{n}}$ processes at time t. The realizations at a given time are denoted with η and $\hat{\eta}^n$. After the predictive density in the normal space has been obtained, it is back-transformed into the original space by applying the inverse NQT.

At this stage we note that the variance given by Eq. (A.8) is a scalar value which is constant over the entire value range of the random variables. This is a consequence of the implicit assumption that the dependency $(\boldsymbol{\eta}, \hat{\boldsymbol{\eta}}^n)$ is homoscedastic. However, for many random variables, such as flow levels, discharges or precipitation, such an assumption is not appropriate. Very low or high flows or water levels in a river can show higher variances than their mid-range. Similar characteristics are observed for precipitation. In such cases it is inaccurate to apply a single linear regression model assuming homoscedastic behaviour. A proven solution is to apply Truncated Normal Distributions (TND), which are fitted to the variables over smaller sub-domains of the whole value range, in which homoscedasticity can be assumed. This approach has been shown [16] to yield satisfactory results in typical situations of heteroscedastic variables with a subdivision of the random variable into two or at most three sub-domains.

Indicator	Def.	CFRS	ERA20C	ERAI	JRA	MERRA	R1	All
correlation	$\rho_{\eta\hat{\eta}_i}$	0.82	0.79	0.89	0.84	0.87	0.81	0.93
var. res.	$1-\rho^2_{\eta\hat{\eta}_i}$	0.32	0.36	0.2	0.28	0.23	0.32	0.14
expl. var.	$\rho^2_{\eta\hat{\eta}_i}$	0.53	0.2	0.74	0.68	0.67	0.63	0.64
frac. var. unexpl.	$\frac{(1-\rho^2_{\eta\hat{\eta}_i})}{\sigma^2_{\hat{\eta}_i}}$	0.38	0.64	0.21	0.29	0.26	0.34	0.17
frac. var. expl.	$\frac{\rho^2_{\eta\hat{\eta}_i}}{\sigma^2_{\hat{\eta}_i}}$	0.62	0.36	0.79	0.71	0.74	0.66	0.83
signal/noise	$\frac{\rho^2_{\eta\hat{\eta}_i}}{(1-\rho^2_{\eta\hat{\eta}_i})}$	1.66	0.57	3.73	2.44	2.87	1.96	4.77
bias		-30.24	-8.94	33.58	38.21	-25.26	-24.25	-2.02
RMSE		47.78	51.5	54.89	69	43.57	51.38	26.31

Table 4: Jhelam, 1979-2005, monsoon season: summary of performance indicators after uncertainty processing for individual models and the combination of all models.

Indicator	Def.	CFRS	ERA20C	ERAI	JRA	MERRA	R1	All
correlation	$\rho_{\eta\hat{\eta}_i}$	0.62	0.66	0.89	0.84	0.74	0.62	0.91
var. res.	$1-\rho^2_{\eta\hat{\eta}_i}$	0.6	0.55	0.2	0.28	0.43	0.59	0.16
expl. var.	$\rho^2_{\eta\hat{\eta}_i}$	0.3	0.09	0.75	0.68	0.53	0.37	0.6
frac. var. unexpl.	$\frac{(1-\rho^2_{\eta\hat{\eta}_i})}{\sigma^2_{\hat{\eta}_i}}$	0.66	0.86	0.21	0.29	0.45	0.61	0.21
frac. var. expl.	$\frac{\rho^2_{\eta\hat{\eta}_i}}{\sigma^2_{\hat{\eta}_i}}$	0.34	0.14	0.79	0.71	0.55	0.39	0.79
signal/noise	$\frac{\rho^2_{\eta\hat{\eta}_i}}{(1-\rho^2_{\eta\hat{\eta}_i})}$	0.51	0.16	3.77	2.39	1.22	0.63	3.69
bias		-6.9	-15.76	8.84	9.42	-17.83	-26.51	-0.7
RMSE		23.75	24.46	18.54	22.47	25.57	33.61	10.36

Table 5: Jhelam, 1979-2005, dry season: summary of performance indicators after uncertainty processing for individual models and the combination of all models.

Subbasin	CFRS	ERA20C	ERAI	JRA	MERRA	NCAR	All Combined
Jhelam	0.69	0.73	0.86	0.82	0.79	0.65	0.9
Middle Indus	0.58	0.75	0.84	0.80	0.79	0.74	0.88
Upper Chenab	0.75	0.79	0.82	0.82	0.83	0.7	0.87
Lower Chenab	0.52	0.69	0.87	0.81	0.77	0.73	0.9
Ravi	0.76	0.76	0.81	0.81	0.8	0.71	0.85

Table 6: Correlations between observations vs. raw predictions ($corr(y, \hat{y}_i)$) and observations vs. posterior conditional mean ($corr(y, E[\mathbf{y}|\hat{\mathbf{y}}^{\mathbf{n}}])$).